Journal of Computational Physics **150,** 549–560 (1999)
Article ID jcph.1999.6206, available online at http://www.idealibrary.com on IDEAL®

The Three Dimensional Non-conforming Finite Element Solution of the Chapman–Ferraro Problem

Petr Klouček*,[1] and Frank R. Toffoletto†,[2]

*Department of Computational and Applied Mathematics, Rice University, 6100 Main Street, Houston, Texas 77005; †Department of Space Physics and Astronomy, Rice University, 6100 Main Street, Houston, Texas 77005
E-mail: kloucek@rice.edu, toffo@rice.edu

Received May 21, 1998; revised November 20, 1998

We demonstrate the feasibility of using a non-conforming, piecewise harmonic finite element method on an unstructured grid in solving a magnetospheric physics problem. We use this approach to construct a global discrete model of the magnetic field of the magnetosphere that includes the effects of shielding currents at the outer boundary (the magnetopause). As in the approach of F. R. Toffoletto *et al.* (1994, *Geophys. Res. Lett.* **21**, 7) the internal magnetospheric field model is that of R. V. Hilmer and G.-H. Voigt (1995, *J. Geophys. Res.*) while the magnetopause shape is based on an empirically determined approximation (1997, J. Shue *et al.*, *J. Geophys. Res.* **102**, 9497). The results is a magnetic field model whose field lines are completely confined within the magnetosphere. The presented numerical results indicate that the discrete non-conforming finite element model is well-suited for magnetospheric field modeling.

Key Words: magnetopause; magnetosphere; Chapman–Ferraro currents; non-conforming finite elements; Laplace's equation; Neumann boundary value problem.

1. INTRODUCTION

The Earth's magnetosphere is formed by the interaction of the solar wind with the Earth's magnetic field. This interaction, to zeroth-order, causes the solar wind to flow around the

[1] This author was partially supported by the National Science Foundation, through the Center for Research on Parallel Computation, under Cooperative Agreement CCR-9120008, and by a grant from the NASA Goddard Space Flight Center.

[2] This author was partially supported by the National Science Foundation (GEM) Grant ATM-9501898 and NASA Grant NAG5-4726.

0021-9991/99 $30.00

cavity carved out by the Earth's magnetic field forming the region known as the magnetosphere. The magnetospheric shape is compressed on the upstream or sunward side and stretched out to form a long tail in the downstream region. This solar-wind magnetosphere interaction produces currents both within the magnetosphere and at the boundary (the magnetopause). The magnetopause currents, often called the Chapman–Ferraro currents [3], confine the magnetospheric magnetic field lines within the magnetosphere in the idealized case of a closed magnetosphere considered here.

Let Ω be a three dimensional domain representing the Earth's magnetosphere, $\partial\Omega$ the boundary, $\partial\Omega_{MP}$ the magnetopause, and $\partial\Omega_{\mathrm{TAIL}}$ be the downstream boundary (so that $\partial\Omega = \partial\Omega_{MP} + \partial\Omega_{\mathrm{TAIL}}$). We define the internal source magnetic field B_S for any $x \in \Omega$ to include (1) the magnetic field of Earth's dipole moment, (2) the tail field generated by currents flowing in the Earth's tail, and (3) the ring current field which is generated by a region of trapped plasma in the near-Earth region. Note that the methods outlined here are general enough to be applicable to any magnetic field model. The Chapman–Ferraro field B_{CF} results from the shielding Chapman–Ferraro current at the magnetopause $\partial\Omega_{MP}$. The total normal component at the magnetopause for a closed magnetosphere is then

$$(B_S(x) + B_{CF}(x)) \cdot n = 0, \qquad x \in \partial\Omega_{MP}, \tag{1.1}$$

where n is the outward unit vector normal to the magnetopause $\partial\Omega_{MP}$. (Details of the Hilmer–Voigt magnetic field model B_S can be found in [5].) By definition, the Chapman–Ferraro field B_{CF} is curl-free in Ω, thus it can be computed as the negative gradient of a scalar potential Φ

$$B_{CF}(x) \stackrel{\text{def}}{=} -\nabla\Phi(x), \qquad x \in \Omega. \tag{1.2}$$

Since the magnetic field B_{CF} is also required to be divergence-free, we have

$$\Delta\Phi(x) = 0, \qquad x \in \Omega. \tag{1.3}$$

The solution of Eq. (1.3) subject to the boundary condition (1.1) is called the Chapman–Ferraro problem [3]. A general discussion of this problem and a review of early work can be found in [23, 13].

A perturbation of this shielding process occurs when there is a small but finite normal component of the magnetic field at the magnetopause [17, 18]. The method we present here is applicable to an arbitrary magnetopause boundary condition and is readily adapted to the open magnetosphere modeling approach introduced in [17]. The open magnetosphere is modeled by replacing (1.1) with a non-homogeneous Neumann boundary condition.

If the magnetopause coincides with one of the coordinate surfaces (e.g., sphere) of a system in which Laplace's equation is separable [11], then Φ may be expanded in harmonic functions of that system and the coefficients may be derived by an inversion integral. Examples include spherical coordinates with a spherical magnetopause [24], parabolic coordinates with a paraboloid-of-revolution magnetopause [1, 15], elliptic coordinates with an ellipsoidal magnetopause [20], and a combination of spherical and cylindrical coordinates with a hemi-spherical dayside magnetopause joined to a semi-infinite cylinder tail magnetopause [22, 24]. While these approaches have provided elegant and useful magnetic field models, the restrictions imposed by the technique limit the class of magnetopause shapes

that can be considered. For example, the magnetopause shape that results from a magnetohydrodynamic (mhd) pressure-balance calculation, where the shocked solar-wind pressure is balanced against the internal magnetic-field pressure, does not generally coincide with any of the shapes for which a separable solution to (1.3) can be found.

An alternative approach for non-separable solutions of (1.3) has been implemented in [16]. The coefficients are fitted to the boundary condition by least squares [16, 21]. A finite difference method has been used in [19] using a curvilinear grid but the technique is restricted to axis-symmetric magnetopause shapes.

The next section describes in detail the technique for solving the Chapman–Ferraro problem using non-conforming finite elements and includes a description of the non-conforming formulation.

2. THE FINITE ELEMENT SOLUTION OF THE CHAPMAN–FERRARO PROBLEM

2.1. *Magnetopause Shape Approximation*

We have taken the Earth's magnetosphere Ω to have the boundary given by the function used in [14]. We approximate the magnetopause $\partial\Omega$ by the function

$$R_{MP} = R_0\left(\frac{2}{1+\cos(\alpha)}\right)^{\beta}, \tag{2.1}$$

where R_0 is a standoff distance, and α is an angle such that $\alpha = 0$ corresponds to the location $(x, y, z) = (R_0, 0, 0)$ (cf. Fig. 1). The parameter β determines the downstream flaring angle of the magnetopause; for simplicity a value of $\beta = 0.5$ is used.

The three-dimensional magnetospheric cavity is generated by a rotation about the x-axis to produce an axisymmetric magnetopause. Non-axisymmetric magnetopause shapes are modeled by making the magnetotail radius R_{MP} a function of the angle φ. For the Earth's

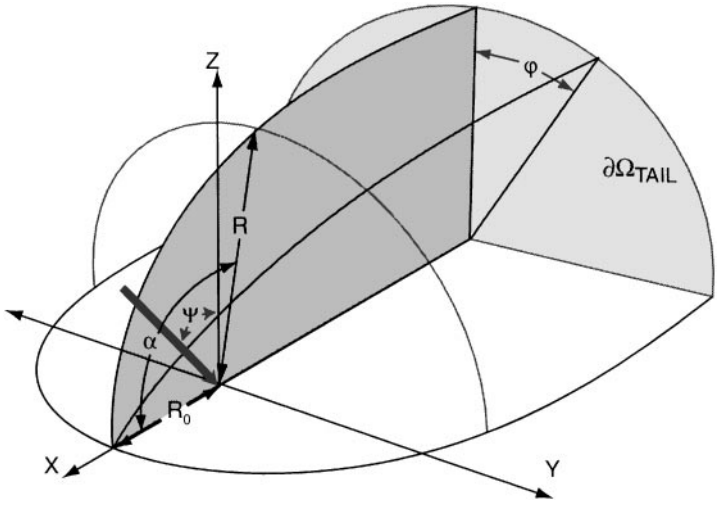

FIG. 1. The geometry and the coordinate system used in this work where x points towards the sun. The angle φ is the cylindrical coordinate out of the $x-z$ plane. In this coordinate system, the Earth's dipole field tilts in the $x-z$ plane at an angle φ. The tail boundary is labeled $\partial\Omega_{\text{TAIL}}$.

magnetosphere, R_0 varies between 8–12 Earth radii (R_E) although during extreme solar wind conditions it can become as small as $4R_E$. For the cases presented here, a constant value of $10R_E$ was used.

2.2. *The Non-conforming Finite Element Formulation*

The definition of a finite element consists of the triplet: (1) the geometry Ω_h, (2) the polynomial space $\mathcal{P}$, and (3) the degrees of freedom Σ; all of these components are described in more detail below. The finite element approximation of the potential Φ of the Chapman–Ferraro magnetic field B_{CF} is based on the spatially averaged non-conforming finite element introduced in [12]. (By definition, conforming finite element spaces consists of a set of functions that are globally continuous while non-conforming finite element spaces contain also discontinuous functions.) This approximation has been extensively used in [6] to approximate almost everywhere discontinuous deformations associated with the Martensitic transformation. The detailed numerical analysis of a generalization of this finite element has been given in [8].

Let Ω be a bounded domain with Lipschitz boundary and let us assume that the necessary compatibility condition for the interior Neumann problem is satisfied, i.e.,

$$\int_{\partial\Omega} B_S \cdot n \, dS = 0, \tag{2.2}$$

as well as

$$\int_{\partial\Omega} B_{CF} \cdot n \, dS = 0. \tag{2.3}$$

We use the following formulation to solve the Laplace's equation (1.1) coupled with the Neumann boundary condition (1.1) using finite elements. The function $\Phi \in W^{1,2}(\Omega)$ is called the *weak solution of the Chapman–Ferraro problem* (1.3) *with the homogeneous Neumann boundary condition* (1.1) if

$$\int_\Omega \nabla\Phi(x)\nabla v(x)\, dx = \int_{\partial\Omega} B_S \cdot n v \, dS, \qquad \text{for any } v \in W^{1,2}(\Omega), \tag{2.4}$$

where $W^{1,2}(\Omega) \stackrel{\text{def}}{=} \{v : \int_\Omega |\nabla v(x)|^2 + |v(x)|^2\, dx < \infty\}$. It is well known that the interior Neumann problem (2.4) has at most one solution and that the solution is determined up to an arbitrary additive constant. The solution can be singled out by assuming any of the conditions $\int_\Omega u(x)\, dx = 0$ or $\int_{\partial\Omega} u \, dS = 0$ or by fixing the solution Φ at some point on $\partial\Omega$.

The application of a non-conforming finite element method is often desirable when the approximated functions or their derivatives are discontinuous or if the approximated functions contain singularities. A priori this approach does not guarantee that the discrete functions would be continuous. The lack of continuity allows a precise approximation of discontinuities and variations that can be concentrated on a very small part of the computational domain. Another advantage of this approach is in the point-wise compliance with various (additional) differential requirements such as the divergence-free condition or local harmonicity.

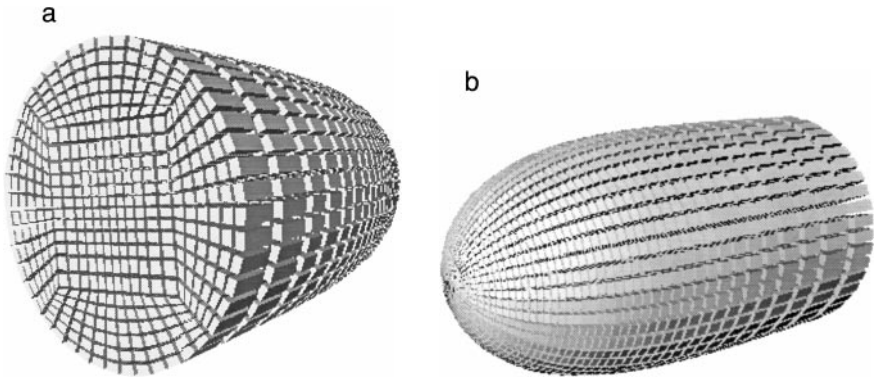

FIG. 2. An illustration of computational domain Ω_h. The left figure highlights the tail of the domain that shows imbedded cubes Q_h. In this figure, each particular element Q_h is shrunk by about 30% to illustrate the partition τ_h.

In order to implement the non-conforming finite element method we partition the computational domain Ω_h into quadrilaterals Q_h such that

$$\Omega_h \stackrel{\text{def}}{=} \bigcup_{Q_h \in \tau_h} Q_h. \tag{2.5}$$

The set τ_h contains all the elements used to reconstruct the domain Ω_h. In particular, we assume that the boundary of the computational domain is piecewise linear. Figure 2 shows the computational domain where each element has been shrunk by 30% to illustrate the partition τ_h.

The *averaged harmonic* finite element we used in our calculations [12, 8] is a polynomial from the finite dimensional space

$$\mathcal{P} = \text{Span}\{1, x, y, z, x^2 - y^2, x^2 - z^2\} \tag{2.6}$$

when restricted to $Q_h \in \tau_h$. We note that

$$-\text{div}\,\nabla p(x, y, z) = 0, \qquad \text{for any } p \in \mathcal{P} \text{ and } (x, y, z) \in Q_h. \tag{2.7}$$

Hence the gradients of these polynomials are divergence-free in every quadrilateral $Q_h \in \tau_h$.

We approximate the potential Φ by the discrete potential Φ_h that is computed by

$$\Phi_h(x, y, z) = \sum_{i=1}^{N_h} \alpha_i v_i(x, y, z), \qquad \text{for any } (x, y, z) \in Q_h,\ Q_h \in \tau_h. \tag{2.8}$$

The functions v_i in (2.8) are polynomials from the polynomial space (2.6) when restricted to any element Q_h. The values at different points of the computational domain Ω_h of these functions are connected by the *averaged weak continuity* condition

$$\int_F v_h|_{Q'_h}\, dS = \int_F v_h|_{Q''_h}\, dS, \qquad \text{for any face } F = \partial Q'_h \cap \partial Q''_h \neq \emptyset,\ Q'_h, Q''_h \in \tau_h. \tag{2.9}$$

We note that this is the weakest condition possible to ensure that a change at one point of Ω_h will effect any other value of a function v_i. Namely, without any additional continuity condition of the type (2.9) we would not be able to implement the boundary conditions.

The possible discontinuity of the approximate potential does not allow us to use the standard gradient operator ∇. We have to extend this operator on a larger class of discontinuous functions. The extension ∇_h is defined with respect to the partition τ_h by

$$\nabla_h \Phi_h(x, y, z) = \nabla \Phi_h(x, y, z) \qquad \text{for} (x, y, z) \in Q_h. \tag{2.10}$$

Thus the extended gradient operator agrees with the standard definition inside any element Q_h. The *discrete gradient operator* ∇_h is defined using one-sided limits on the boundary of Q_h and it ignores the effect of discontinuities along ∂Q_h.

The non-conforming finite element formulation of (2.4) reads: *Find* $\alpha_i \in \mathbb{R}$, $i = 1, 2, \ldots, N_h$, *such that*

$$\sum_{i=1}^{N_h} \sum_{j=1}^{N_h} \alpha_i \int_{Q_j} \nabla v_i(x, y, z) \nabla v_k(x, y, z)\, dx = \int_{\partial \Omega_h} B_S \cdot n v_k \, dS,$$

$$\text{for any } k = 1, 2, \ldots, N_h. \tag{2.11}$$

All operations involving integrals of various quantities are done on a parent finite element which in this case is a unit cube. The partition Q_h is mapped onto the unit cube (using trilinear mapping) and all integrals are done using substitution. Each Q_h has a fixed number of degrees of freedom (DOF) and polynomial space $\mathcal{P}$ associated with it. The mapping process does not guarantee that these quantities are preserved [4]. In our case, since the DOF are the integrals over the faces of Q_h this quantity is preserved but the polynomial space is not. In other words, the mapping required to map the unit cube onto any of the elements $Q_h \in \tau_h$ does not preserve the polynomial space $\mathcal{P}$ in which we are approximating the potential Φ. By computing appropriate scaling factors, $\mathcal{P}$ can be preserved. However, calculations with and without these scaling factors showed similar results which suggests that this deficiency does not introduce an additional error beyond the $\mathcal{O}(h)$ precision associated with the non-conformity of the approximation.

2.3. *Boundary Conditions*

As mentioned in the Introduction the boundary of the computational domain Ω is divided into two parts: $\partial\Omega_{MP}$ and $\partial\Omega_{\text{TAIL}}$. The applied Neumann boundary condition, as required to satisfy (2.3), is

$$B_{CF}(x) \cdot n = -B_S(x), \qquad \text{for } x \in \partial\Omega_{MP} \tag{2.12}$$

while on the tailward boundary ($\partial\Omega_{\text{TAIL}}$) we make the simplifying assumption that the normal component (B_{TAIL}) on $\partial\Omega_{\text{TAIL}}$ is constant and is defined by

$$B_{CF}(x) \cdot n = B_{\text{TAIL}} = \frac{\int_{\partial\Omega_{MP}} B_S \cdot n \, dS}{\text{meas}(\partial\Omega_{\text{TAIL}})}, \qquad x \in \partial\Omega_{\text{TAIL}}, \tag{2.13}$$

where meas($\partial\Omega_{\text{TAIL}}$) is the cross-sectional area of the region $\partial\Omega_{\text{TAIL}}$. The formula (2.13) ensures that (2.3) is satisfied.

3. RESULTS

3.1. *Calculations with Zero Tilt*

Computation of the magnetic field with zero tilt (i.e., when the source magnetic field B_S points in the direction $(0, 0, -1)$) constitutes a mathematically and physically simpler problem. In this case, $\int_{\partial\Omega_{MP}} B_S \cdot n\, dS = 0$ so that Eq. (2.13) results in the simple boundary condition $B_{CF}(x) \cdot n = 0$ for all $x \in \partial\Omega_{\text{TAIL}}$. This condition states that at a sufficiently distant downstream location the solution Φ is independent of downstream position (i.e., $\partial\Phi/\partial x = 0$).

The solution was implemented using a three-dimensional version of the finite element analysis tool (FEAT) [2]. The calculations used a low spatial resolution to provide sufficient computational evidence of the efficiency of the method. Namely, we take the x-direction resolution h_x to be $80/21$, and $h_y = h_z \sim 40/12$, measured at the diameter of Ω_h. As expected, calculations with a finer grid produced similar results to the ones shown here but were substantially more expensive. The numerical integration associated with evaluation of the variational integrals in (2.11) is done using a Hammer and Stroud cubature formula that is accurate up to polynomials of order 5. The partition τ_h in combination with the presented finite element and high-order numerical integration yields a system matrix A_h representing the system (2.11) with low condition number. (A lower order integration scheme yielded matrices with higher condition numbers.)

The discrete weakly harmonic solution to (2.11) must be symmetric. The fieldlines are computed using an Euler integration routine with adaptive stepsize. The result is shown in Fig. 3 which represents the $x - z$ view of the computed fieldlines. One of the important tests of the solution Φ_h is to check if the fieldlines corresponding to $\nabla\Phi_h$ which originate in a plane stay in this plane. The non-conforming approximation allows for a lot of freedom in this sense. The fieldlines stay within a range of $y = \pm 0.05$ except for

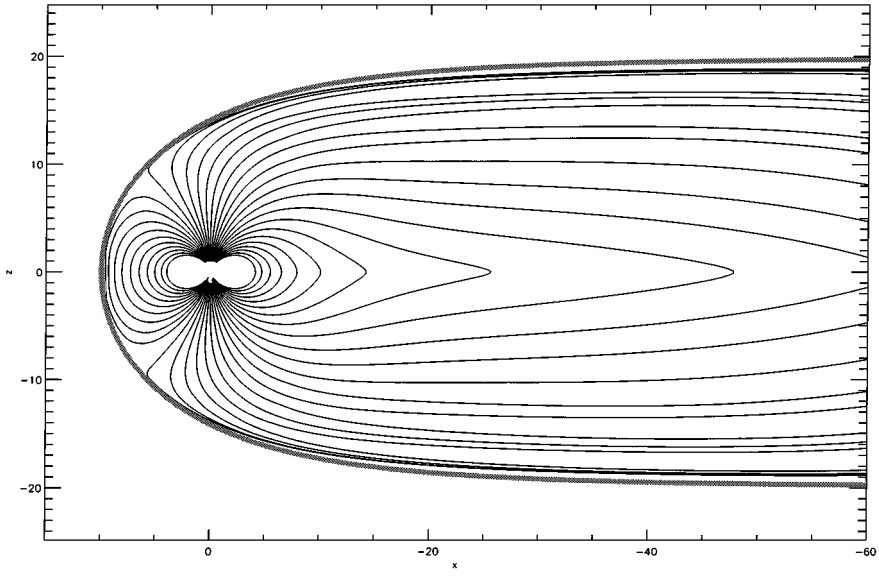

FIG. 3. The fieldlines given by the computed solution $\nabla\Phi_h$ in the $x - z$ plane. The outer heavy line represents the magnetopause location.

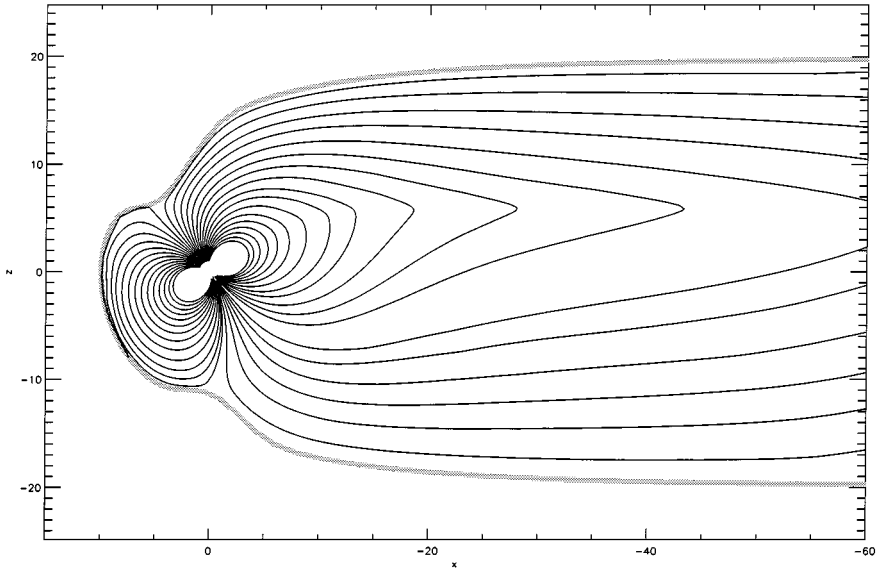

FIG. 4. The fieldlines corresponding to the dipole field tilted by 35°.

the fieldlines that pass extremely close to the singularity in B_s. This means that lateral approximation error is about 0.1% which is well beyond the y-direction resolution $h_y \sim 3\frac{1}{3}$. The lateral numerical stability seems to be a consequence of the point-wise harmonicity of the spatial approximation. We also computed solutions using a conforming element, but solutions of similar accuracy to the non-conforming element proved more difficult to achieve.

3.2. *Calculations with Nonzero Tilt*

When the dipole tilt angle ϕ is nonzero we have

$$\int_{\partial\Omega_{MP}} B_S \cdot n \, dS \neq 0 \tag{3.1}$$

in Eq. (2.13), resulting in a nonzero value for the normal component on $\partial\Omega_{\text{TAIL}}$ in (2.3).

An example of a magnetic field configuration where the dipole field is tilted by 35° is shown in Fig. 4. A three-dimensional perspective plot is shown in Fig. 5. Note that for nonzero tilt the Hilmer–Voigt magnetic field model also displaces the tail field off the $x - y$-plane. In both figures the heavy lines denote the location of the magnetopause.

3.3. *Calculations with a Non-axisymmetric Magnetopause*

A further application of our discrete model is the computation of a configuration where the magnetopause shape is no longer axisymmetric. In this case, the methods described in the previous section are the same with the exception that meas($\partial\Omega_{\text{TAIL}}$) becomes the cross-sectional area of $\partial\Omega_{\text{TAIL}}$. Pressure balance considerations indicate that the magnetopause should be indented in a region where the magnetic field is a minimum (the cusp); such an indentation has been modeled and is shown in Figure 6. The resulting field line configuration is shown in Figs. 7 and 8. Figure 8 shows that the y-extent has been compressed.

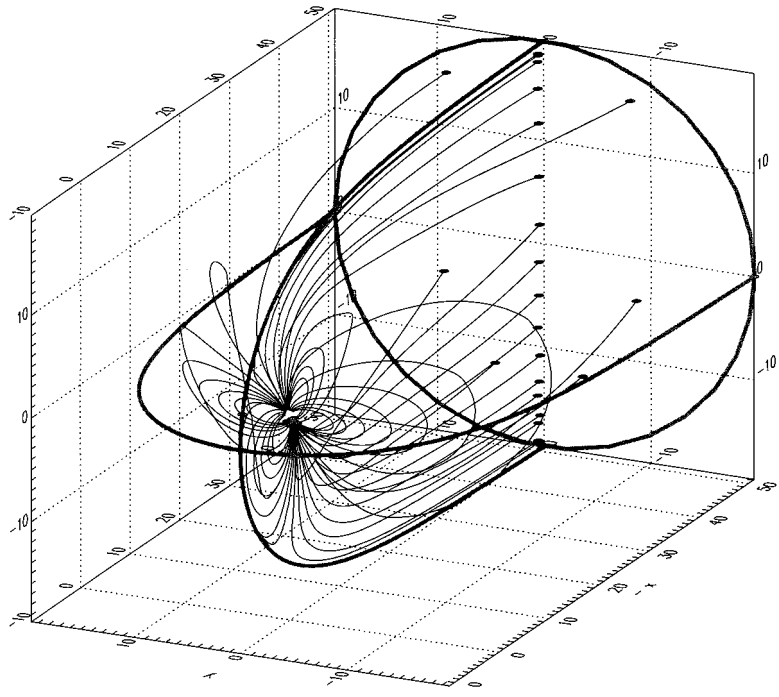

FIG. 5. Three-dimensional plot of the final field configuration for the tilted dipole field. The heavy lines illustrate the location of the magnetopause.

4. SUMMARY AND CONCLUSIONS

We have used a non-conforming finite-element method to generate a discrete magnetospheric field model. This type of technique is a generalization and extension of previous work with a variety of possible applications in magnetospheric modeling. The numerical calculations indicate that non-conforming finite elements can be successfully used to

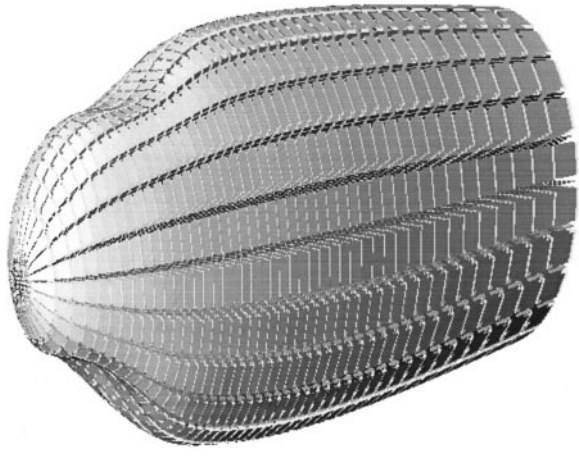

FIG. 6. Grid configuration for the case of a non-axisymmetric magnetopause.

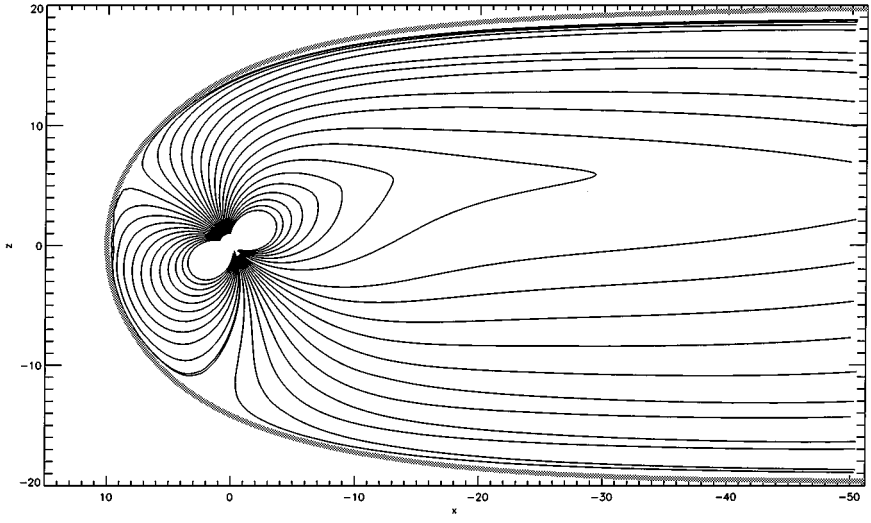

FIG. 7. Fieldline plots as viewed in the $x-z$ plane for the case of a non-axisymmetric magnetopause; the indentations were placed near the local minimum in the magnetic field, the location of which is asymmetric with respect to z. The outer-heavy line represents the magnetopause location.

approximate continuous quantities. The resulting method presented in this paper proves to be robust and to a large extent independent of the underlying unstructured grid. The local harmonicity of the finite elements used in our calculations proves to be useful in maintaining the symmetry of the solution even close to the singularity.

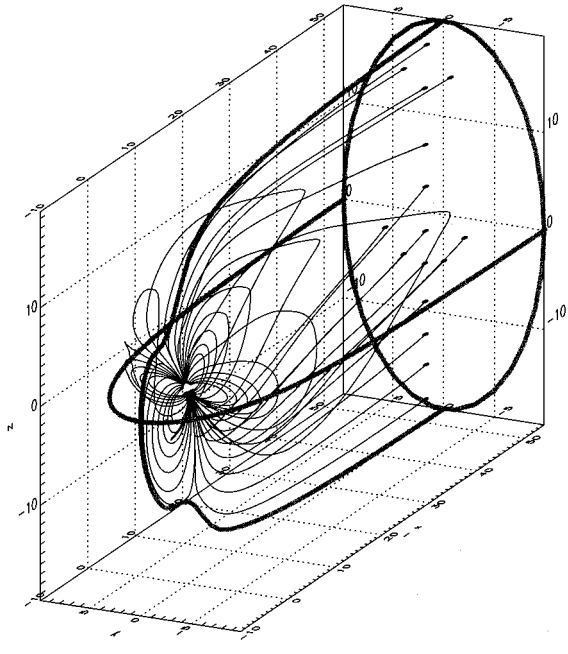

FIG. 8. Fieldline plots as viewed in a three-dimensional perspective plot for the case of a non-axisymmetric magnetopause. The outer-heavy line represents the magnetopause location. The indentations are placed near minima in the internal magnetic field.

Our discrete method can be used to extend and generalize empirically based magnetic field [21] and theoretical models [18] by allowing arbitrary magnetopause shapes to be used in calculations. The results presented in this paper provide evidence that possible lack of continuity does not play an important role when the approximated field quantities are smooth. This observation leads us to believe that the non-conforming finite element method described in this work will be a valuable tool for the approximation of the MHD equations that contain mixture of difficulties such as discontinuities, and divergence-free as well as smooth field quantities. The application of a spatially non-conforming approximation using finite elements provides a simple tool for simultaneous treatment of the difficulties mentioned above.

REFERENCES

1. I. I. Alekseev and V. P. Shabansky, A model of a magnetic field in the geomagnetosphere, *Planet. Space Sci.* **20**, 117 (1972).
2. H. Blum, J. Harig, and S. Muller, FEAT: Finite element analysis tools, release 1.0, user manual preprint 554, University of Heidelberg, January 1990.
3. S. Chapman and V. C. A. Ferraro, A new theory of magnetic storms, *Nature* **126**, 129 (1930).
4. K. Eriksson, D. Estep, P. Hansbo, and C. Johnson, *Computational Differential Equations* (Cambridge Univ. Press, Cambridge, UK, 1996).
5. R. V. Hilmer and G.-H. Voigt, A magnetospheric magnetic field model with flexible current systems driven by independent physical parameters, *J. Geophys. Res.* (1995).
6. P. Klouček and M. Luskin, The computations of the dynamics of the Martensitic deformation, *Continuum Mech. Thermodyn.* **6** (1994).
7. P. Klouček and M. Luskin, Computational modeling of the Martensitic transformation with surface energy, *Math. Comput. Model.* **20**(10/11), 101 (1994).
8. P. Klouček, B. Li, and M. Luskin, Non-conforming finite element approximation of the microstructure, *Math. Comp.* **65**(215) (1996).
9. D. K. Koitchev, M. S. Kaschiev, and M. D. Kartelev, Finite element numerical modeling of stationary two-dimensional magnetosphere with defined boundary, *J. Comput. Phys.* **119**, 220 (1995).
10. M. D. Kartelev, M. S. Kaschiev, and D. K. Koitchev, Simplified 3D magnetospheric field, *J. Comput. Phys.*, in press.
11. P. Moon and D. E. Spencer, *Field Theory Handbook* (Springer-Verlag, New York/Berlin, 1988).
12. R. Rannacher and S. Turek, Simple non-conforming quadrilateral Stokes element, *Numer. Methods Partial Differential Equations* **8** (1992).
13. G. L. Siscoe, The magnetospheric boundary, in *Physics of Space Plasmas*, edited by T. Chang, G. B. Crew, and J. R. Jasperse (Scientific Publishers, Cambridge, MA, 1988), p. 3.
14. J. Shue, J. K. Chao, H. C. Fu, C. T. Russell, P. Song. K. K. Khurana, and H. I. Singer, A new functional form to study the solar wind control of the magnetopause size and shape, *J. Geophys. Res.* **102**, 9497 (1997).
15. D. P. Stern, Parabolic harmonics in magnetospheric modeling: The main dipole and the ring current, *J. Geophys. Res.* **90**(13), 10,851 (1985).
16. M. Schulz and M. C. McNab, Source-surface model of the magnetosphere, *Geophys. Res. Lett.* **14**, 182 (1987).
17. F. R. Toffoletto and T. W. Hill, Mapping of the solar wind electric field to the Earth's polar caps, *J. Geophys. Res.* **94**, 329 (1989).
18. F. R. Toffoletto and T. W. Hill, A non-singular model of the open magnetosphere, *J. Geophys. Res.* **98**, 1339 (1993).
19. F. R. Toffoletto, R. V. Hilmer, T. W. Hill, and G. H. Voigt, Solution of the Chapman–Ferraro problem with an arbitrary magnetopause, *Geophys. Res. Lett.* **21**, 7 (1994).

20. N. A. Tsyganenko, A solution of the Chapman–Ferraro problem for an ellipsoidal magnetopause, *Planet. Space Sci.* **37**, 1037 (1989).
21. N. A. Tsyganenko, Modeling the Earth's magnetospheric magnetic field confined within a realistic magnetopause, *J. Geophys. Res.* **100**, 5599 (1995).
22. G.-H. Voigt, A three dimensional, analytical magnetospheric model with defined magnetopause, *Z. Geophys.* **38** (1972).
23. G. H. Voigt, Magnetospheric equilibrium configurations and slow adiabatic convection, in *Solar Wind-Magnetosphere Coupling*, edited by Y. Kamide and J. A. Slavin (Terra Scientific, Tokyo, 1986), p. 233.
24. G.-H. Voigt, A mathematical magnetospheric field model with independent physical parameters, *Planet. Space Sci.* **1**, 29 (1981).